Electronic Supplementary Material (ESI) for Physical Chemistry Chemical Physics.

ELECTRONIC SUPPLEMENTARY INFORMATION (ESI)

Protein-Protein Interactions within Photosystem II under Photoprotection: The Synergy between CP29 Minor Antenna, Subunit S (PsbS) and Zeaxanthin at all-atom resolution

Vangelis Daskalakis[1*]
[1]Department of Environmental Science and Technology, Cyprus University of Technology, 30 Archbishop Kyprianou Str., 3603, Limassol, Cyprus. *Correspondence and requests for materials should be addressed to V.D. (email: evangelos.daskalakis@cut.ac.cy, tel: +357 25002458, fax: +357 25002820)

1 Protein-Xanthophyll interactions within micelles

In the confined space of a ligand-enriched nanodisc, or micelle (**Fig. S1 A-C**), the protein-ligand interactions are enhanced and in addition the integral proteins may be conformationally locked, as a recent study for PSI has showed.[1] By employing this lipid bilayer (membrane) analogue as starting structure, unbiased protein-ligand interactions can be probed in the classical MD scheme within the ns-time scale. Taking protein-micelle models as the starting point, PsbS and CP29 conformations have been produced in the classical MD scheme (310K), at semi-isotropic pressure coupling to enable micelle-to-nanodisc/ lipid bilayer transition,[2] (**Fig. S1 A** to **B**) in the presence also of Vio, or Zea (ligands) inside an initial micelle phase (**Fig. S1 C**). This transition enables both the efficient orientation of the lipids around the hydrophobic protein regions and the correct hydration of the hydrophilic regions by the aquatic phase.[3] Furthermore, it samples realistic aggregations of long-chain lipids[2] and enhances protein-xanthophyll interactions. We therefore, can consider these conformations as analogues to the dynamics of the integral PsbS, or CP29 in membranes enriched with the same xanthophylls. In **Fig. S2 A** the Solvent Accessible Surface Area (SASA) for PsbS and CP29 is compared between micelle- and membrane- embedded conformations, based on the classical MD trajectories. We can observe both an around 8% decrease and a narrowing of the SAS probability density for the CP29 SASA that is confined within a micelle. This can be consistent with a conformational locking within the micelle, in line with experimental evidence.[1] To the contrary, the respective PsbS SASA is not disturbed significantly by the confinement within the micelle, which might be attributed to the absence of bulky pigments (Chlorophylls).

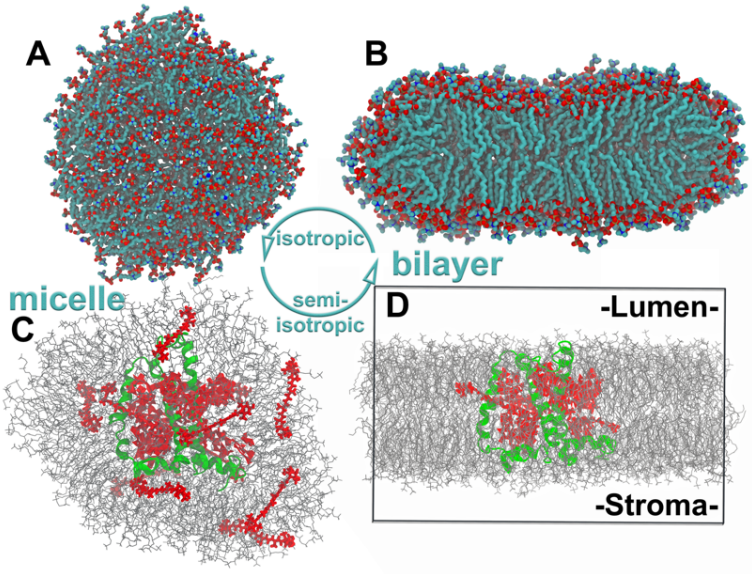

Figure S1 | Lipid structures **A.** A lipid micelle structure in an aquatic phase at the end of a 250ns production run with isotropic pressure coupling at the isothermal-isobaric ensemble. Head groups are shown in red and tails in grey. **B.** A lipid bilayer-like/ nanodisc structure in an aquatic phase formed from the micelle (**A**) at the end of a 250ns production run with semi-isotropic pressure coupling at the isothermal-isobaric ensemble. **C.** CP29 protein (green cartoon) embedded in a micelle (grey lines). Red structures refer to the pigments (chlorophylls, or carotenoids). **D.** CP29 protein (green cartoon) embedded in a lipid bilayer membrane (grey lines). Red structures refer to the pigments (chlorophylls, or carotenoids). Water molecules have been removed from all structures for clarity.

The CP29/ PsbS – ligand (Vio, Zea) occupancies per residue are depicted in **Fig. S2 B** and are based on micelle confined conformations-dynamics (**Fig. S1 C**). The occupancies refer to residue-ligand interactions that hold throughout the production trajectories (value of 1), partially (0-0.99), or are absent (value of 0). Most of the interactions reach values of unit occupancy (**Fig. S2 B**), thus it is noted that by employing this protein confinement method in a micelle, an efficient sampling of protein-ligand interactions is achieved and the residue dynamics within the protein should adapt to the presence of a ligand. This is an analogue to the changes within the thylakoid membrane composition during the xanthophyll cycle. A preference of Zea for the monomer A (PsbS-A) of PsbS, and to the contrary, a preference of Vio for PsbS-B is evident. PsbS-A and PsbS-B refer to chain A and B respectively as defined in the PsbS crystal structure.[4] The preferences seem complementary for the regions of the PsbS in terms of Zea, and Vio ligation. The specificity of Zea/ Vio ligation to either PsbS PsbS-A, or B was also identified in trajectories of our previous study,[5] employing a completely different approach to probe ligation, however the results were averaged for the two PsbS monomers and thus the ligation specificity was not discussed therein. For CP29 we observe that interaction with Zea is taking place at more binding sites, compared to Vio (**Fig. S2 B**).

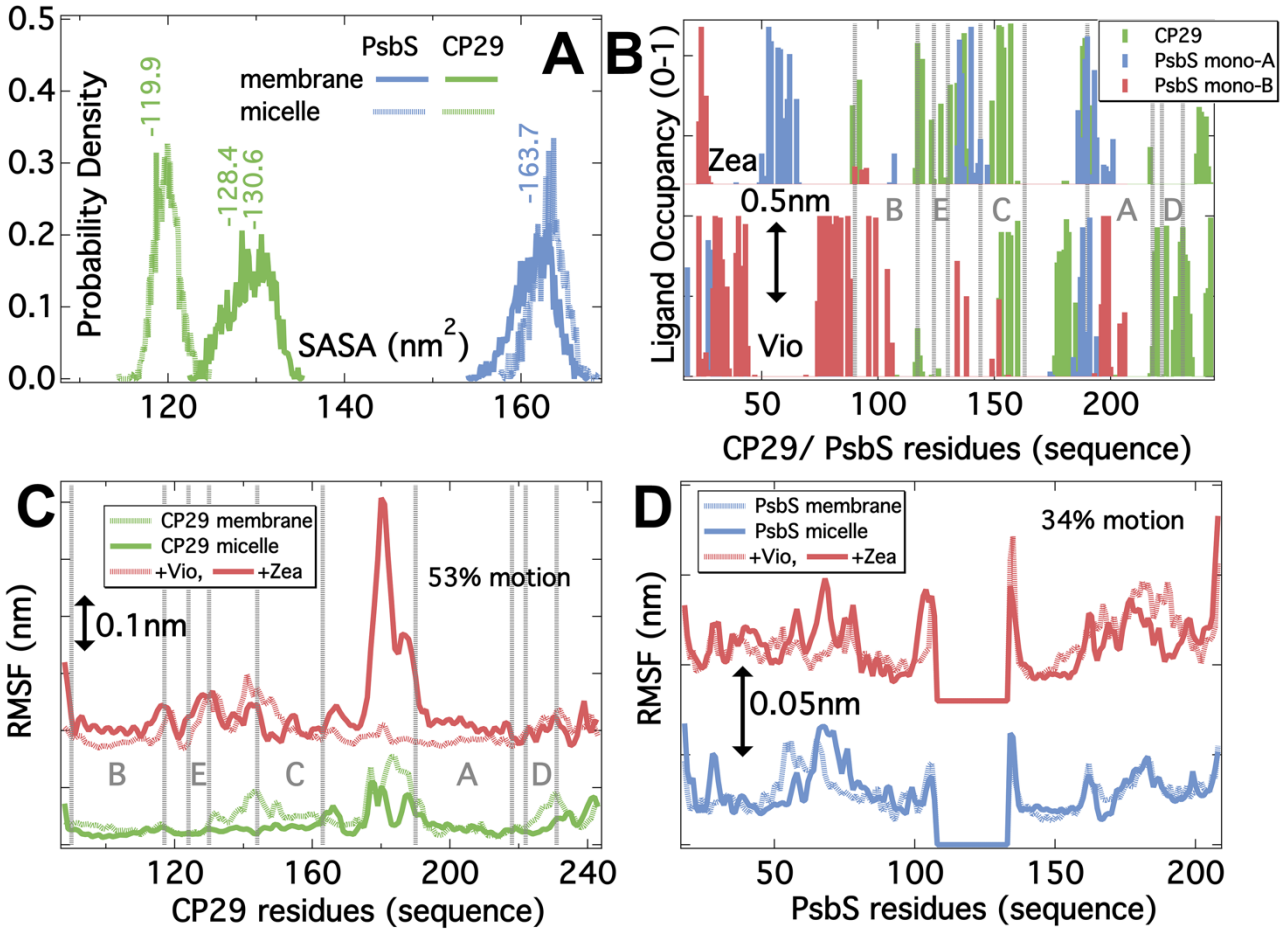

Figure S2 | The protein – ligand interactions. **A.** Comparison between the Solvent Accessible Surface Areas (SASA) for CP29 and PsbS in a lipid micelle, or bilayer membrane. **B.** Xanthophyll (Vio – Violaxanthin, and Zea – Zeaxanthin) occupancies per residue in the interaction with CP29 or PsbS. The CP29 helices (HA, HB, HC and HD) are indicated in the sequence for reference. **C-D.** The Root Mean Square Fluctuations (RMSF) per residue for the CP29 (**C**) and PsbS (**D**) proteins in micelles and the presence of Vio-Zea, or within a lipid bilayer membrane.

In the same context, the Root Mean Square Fluctuations (RMSF) per residue are depicted for CP29 and PsbS based on the dynamics of the proteins inside a membrane, inside a micelle, and in the interaction with the xanthophylls inside a micelle (**Fig. S2 C-D**). The analysis is based on essential dynamics[6] and refers to 53 and 34% contributions to the overall CP29 and PsbS protein motions, respectively. For the essential dynamics, or PCA[6] it is made sure that the presented results (i.e. average Root Mean Square Fluctuations – RMSF) are compared between samples where the sum percentage (%) contribution to the overall motion, of the chosen number of principal vectors,

is the same. Usually to achieve this, between 3-7 vectors are used per case. For the CP29-bilayer, or CP29-micelle systems this adds to 53% contribution to the overall motion, while for the PsbS-bilayer, or PsbS-micelle systems, this sums to 34% contribution. RMSF calculation leads also to the estimation of the B-Factors.

The conformational locking, only for the CP29, is evident also in the RMSF graphs, where lower RMSF values are recorded for the micelle confined state, compared to the integral membrane conformation. To the contrary, RMSF values of similar magnitude are recorded for PsbS embedded both in a membrane, or a micelle. An effective interaction between protein-ligands is observed for both CP29 and PsbS. Comparing the red curves in **Figs. S2 C-D**, we can observe that CP29 responds strongly to the presence of the xanthophylls (especially Zea), whereas PsbS-xanthophyll interaction appears to have, on the average (PsbS-A, B), a relatively less of an effect on the PsbS residue dynamics within the micelle. However, this latter does not in any case imply a weak, nor an unimportant interaction, as it refers to the averaged monomer response. The response of PsbS-A to Zea ligation is enhanced, compared to the PsbS-B response, as expected, in line with the Zea-PsbS-A interaction preference, but the average response seems reduced. In any case, the protein-ligand occupancies per residue presented in **Fig. S2 B** are consistent with a change in the RMSF values per the respective residue for both CP29 and PsbS (**Figs. S2 C-D**). Changes in RMSF fluctuations upon ligand binding, are thus localized within the protein-ligand interaction sites.

2 Methods

2.1 The CP29–PsbS Docking (*equilibrium*).

Central structures of CP29, or PsbS were extracted from the single protein-micelle production trajectories (last 150ns) using the clustering single-linkage method in GROMACS[7] with a cut-off at 0.1nm. The latter employs the criterion of the RMSD of protein Ca atoms as the distance between structures at a cutoff value of 0.1nm. From the related clusters, the central structure of the most populated cluster was chosen as a representative conformation of each protein state.

These structures are subsequently deprived of pigments, water, ions, or lipids and fed as different PsbS-CP29 pairs to the ClusPro protocol[8] which was employed on rigid protein structures with hydrophobic interactions to be favoured for the docking. Due to the lack of universal force fields for the online docking servers, like ClusPro,[8] and the widely used Haddock,[9, 10] pigments in LHCs pose a drawback on the parametrization. Hence, their initial removal from the LHCs is necessary. However, due to the rigid-based docking protocol of the ClusPro, contrary to the flexible-docking of Haddock, the LHCs structures remain intact and close to their crystallographic, or ensemble (MD) central conformations. All possible PsbS-CP29 pair combinations, coming from within POPC-only, POPC-Vio, or POPC-Zea containing micelles, were assumed. For details on ClusPro parametrization, please refer to a previous successful adaptation for the PsbS-LCHII docking poses, based on PsbS-membrane, and major LHCII-membrane systems.[5] Numerous PsbS-CP29 docked structures were thus produced. In line with a previous study,[5] only the structures coming from PsbS/ or CP29 micelles enriched with Zea give an acceptable complex interaction at the correct lumen-stroma orientation. This acceptable orientation was used as a guiding map. In detail, the initial CP29 and PsbS prepared structures that contained all pigments and crystallographic waters (prior to equilibration, based on crystal structures, *see sample preparation in the main manuscript*) were aligned with the PsbS-CP29 ClusPro docking pose, using the MultiSeq[11] protocol in VMD 1.9.3.[12] The PsbS-CP29 distance was increased in the restructured docked complex, compared with the ClusPro prediction, in order to avoid steric clashes between the CP29 pigments and PsbS residues.

The restructured complex was embedded in a lipid bilayer membrane as in the cases of isolated CP29, or PsbS (*see sample preparation, in the main manuscript*), the system was equilibrated and two independent classical MD production trajectories (250ns each, 0.5μs total) were produced. Upon comparison between the initial and final structures, no major conformational changes were introduced, which positively evaluates the complex structure and ensures a well-predicted complex. The final equilibrated structures (at 250ns) of the PsbS-CP29 complex were extracted from the previous production trajectories. These structures were used as input for the dissociation-association energetics of the PsbS-CP29 complex. A central structure of the complex was additionally extracted out of these trajectories by employing the single-linkage clustering method in GROMACS[7] with a cut-off at 0.1nm and fed to the RING protocol.[13] The clustering employs the criterion of the RMSD of protein Ca atoms as the distance between structures at a cutoff value of 0.1nm. From the related clusters, the central structure of the most populated cluster was chosen as a representative conformation of the PsbS-CP29 complex state. RING identified interacting nodes between PsbS-CP29 Ca atoms (**Fig. 1D** *in the main manuscript*), with the default parametrization for strict distance thresholds (0.35nm for hydrogen bonds, 0.05nm for van der Waals interactions, 0.4nm for salt bridges, and 0.65nm for π-π stacking or π-cation interactions).

2.2 Dissociation-Association Energetics (*out-of-equilibrium*)

Free Energy Profiles (FEP) from metadynamics. To compute the FEP of associating-dissociating the integral membrane PsbS-CP29 complex, a combination of SMD[14, 15] and metaD[16, 17] runs was employed. The GROMACS 5.1.4[7] engine, along with PLUMED 2.3.1[18] was used for this batch of runs. The SMD runs were performed at 310K with the same parameters as in classical (equilibrium) MD, by employing a *repulsive* pulling force between the center of masses (CoM) of (i) the PsbS monomers (Ca protein atoms), without the presence of CP29, (ii) the PsbS monomers (Ca atoms) in the presence of CP29, and (iii) the PsbS dimer (Ca atoms) and the CP29 (Ca atoms). For the first (i) case the initial structure was extracted at the end of the PsbS-bilayer system classical MD production trajectories, while for the rest (ii, iii) of the cases, the initial structure was extracted at the end of the classical MD production trajectories of the ClusPro based and reconstructed PsbS-CP29 docked complex (*see above*). For the PsbS dimer-to-monomer dissociation the CoMs distance was fluctuating from around 2.0 to 6.0nm (cases i, ii), and for the PsbS-CP29 dissociation, the CoMs distance was fluctuating from around 3.0 to 7.0nm. The structures by the end simulation time were again fed into a second round of SMD trajectories, but in this case employing an *attractive* pulling force between the same CoMs for association. For all previous SMD runs, the force on the CoMs was increased between 0-1000 kJ mol^{-1} nm^{-2} over 10ns, then a constant force (1000 kJ mol^{-1} nm^{-2}) was applied for a period of 100ns, and then the force was gradually reduced to zero, over the next 90ns. The SMD runs, summed to a total of 1.2μs sampling. In addition, metaD runs at 310K were initiated at structures extracted along the repulsive-attractive SMD trajectories when the CoMs were at around 2.0, 4.0, or 6.0nm apart (cases i, ii), and 3.0, 5.0, or 7.0nm apart (case iii). The distance between the respective CoMs was set as a single collective variable (CV). The CoM was again calculated based on the Ca atoms. A path CV is formed that involves the distance α (2.0 nm < α < 6.0 nm, or 3.0 nm < α < 7.0 nm) along a reference path between dissociation-association states. For a few trajectories, the metaD sampling had to be extended beyond 6.0 or 7.0nm as the distance of the COMs fluctuated beyond the pre-set values. The grid (distance) resolution was set at 0.1nm. The bias was achieved by depositing Gaussians every 1ps, of widths that cover the space of 500 time-steps in the CV space. The starting Gaussian height was at 1.4 kJ/mol and it was gradually decreased in terms of a diffusive adaptive bias scheme with a temperature difference of ΔT=3410K (well-tempered metaD bias factor 12). This setup achieves sampling of the fine-details of the free energy profile and it is based on numerous test-runs with variant values of the bias factor, Gaussian width and height, that were performed, but lead to similar results and no additional information. In detail, metaD trajectories, were also initiated from the complexed proteins at equilibrium (prior to SMD), but were run with a Gaussian height of up to 5.0 kJ/mol and a bias factor of up to 25. All metaD runs were performed with the same parameters as in classical (equilibrium) MD, for 200ns each trajectory. This totalled in around 6.0μs of metaD runs. The structures that fell within the basins (free energy minima) were clustered using the default GROMACS algorithm for clustering. The latter employs the criterion of the RMSD of protein Ca atoms as the distance between structures at a cutoff value of 0.1nm. From the related clusters at the energy minima, the central structure of the most populated cluster was chosen as a representative conformation of the PsbS-CP29 complex state at each basin.

All reaction coordinates (CVs) employed are based on the distances between the CoMs of individual monomers, or proteins. The stability of the PsbS monomers (A, B) and of CP29 throughout the metaD biased dynamics of PsbS-CP29 dissociation-association, can be judged by their Ca Root Mean Square Deviation (RMSD) values. The RMSD values fall below 0.25nm, indicating stability over 200ns long trajectories. The RMSD values are shown in **Fig. S3** averaged over all metaD trajectories of the different reaction coordinates (CVs). The shaded areas around the RMSD lines are representatives of the error bars (standard deviation) out of the averaging.

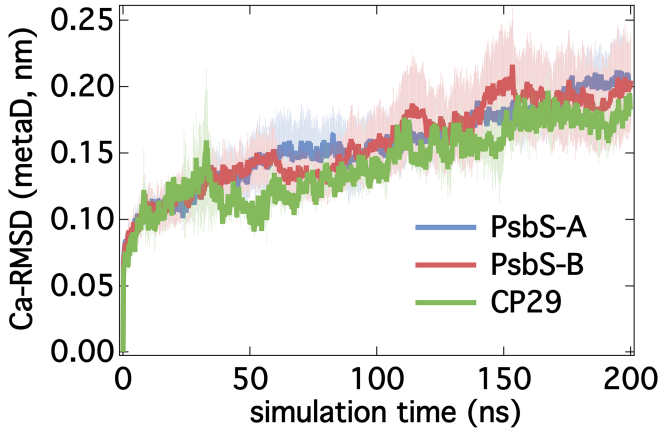

Figure S3 | The Root Mean Square Deviations (RMSD) of the Ca atoms of the PsbS monomers (A, B) and CP29 as averaged over all the Metadynamics (metaD) runs (around 6.0μs trajectories). The shaded areas reflect the standard deviation from the averaging.

Potential of Mean Force (PMF) from steered MD. To compute the PMF[14, 15] of associating-dissociating the PsbS-CP29 complex, a different setup of SMD runs was employed. The calculated work from the SMD runs, can be associated with the PMF based on the formulation by Cuendet et al. and Schulten via the cumulant expansion method[14,

[15] Numerous dissociation trajectories need to be run for this case and thus, for the computational efficiency, the PsbS-CP29 complex was deprived of its lipid-bilayer/ aquatic environment, but left within the same unit cell size as the integral protein membrane systems, and the equations of motion were based on Langevin Dynamics[19] with a friction coefficient of 5 ps^{-1} for all non-hydrogen atoms[20] at the NVT (isothermal) ensemble. This accounts for friction (implicit membrane-aquatic phase)[20] and random noise.[14, 20] Initial PsbS-CP29 complex structures, for the Langevin SMD, were extracted along the classical MD (*equilibrium*) production trajectories of the integral membrane PsbS-CP29 restructured complex based on the ClusPro prediction (sampling every 10ns after the first 100ns). This ensures the correct initial orientation of the complex, with its principal axis aligned to the z-axis of the unit cell. A simulation time of 35ns per SMD trajectory was chosen for 32 independent runs per pulling case (i, ii, iii). The systems were equilibrated between 0-4ns, then the force on the CoMs was increased between 0-1000 kJ mol^{-1} nm^{-2} over 6ns, then a constant force (1000 kJ mol^{-1} nm^{-2}) was applied for a period of 25ns. For these runs, and to avoid the relative rolling of the complexed proteins or monomers,[15] due to the absence of a lipid bilayer membrane, the Ca atoms of each protein were divided in two groups based on their relative position on the z-axis: above or below the CoMs of each protein, or monomer. The pulling force was separately applied on the CoMs of each group of atoms. The latter ensures the correct dissociation of the complex, whereas in the case of a pulling force on the overall CoMs of each protein, or monomer, the proteins roll in relation to each other, instead of fully dissociating. The large number of trajectories per pulling case provides the adequate statistics to compute energetic observables for the complex, by averaging usually large fluctuations and ensuring independence on initial conditions. A weak restraint (100 kJ mol^{-1} nm^{-2}) was applied on the z-axis motion only, for the overall CoMs of the PsbS/ CP29 proteins, or PsbS monomers, to make sure we have no movement along the z-axis. This restraint is perpendicular to the reaction coordinate (pulling force) and thus it does not accumulate work, or affect the calculated PMF, but inhibits rotation around the protein axes, or relative rolling that could lead to artefacts.[15] In this way, the proteins behave as being embedded in a lipid bilayer membrane.

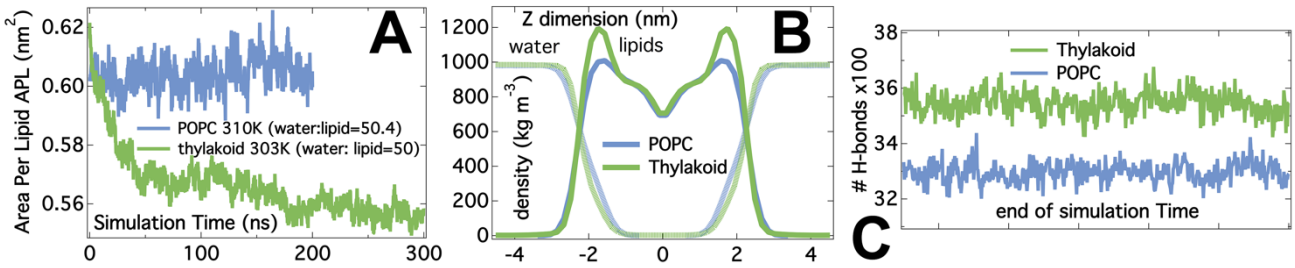

Figure S4 | Comparison between the POPC (OPLS-AA) and native thylakoid lipid-based (AMBER) membranes. **A.** The area per lipid (APL) convergence. **B.** The partial densities for lipids and water. **C.** The number of hydrogen bonds (H-bonds) between lipids and the aquatic phase (water).

3 Micelle-confined versus integral and native membrane protein conformations

Enhanced sampling methods for protein-ligand interactions, like the aforementioned SMD scheme, have been previously applied for an integral membrane PsbS model.[5] However, a biasing potential needed to be employed, the computational cost was very high and the results are sometimes heavily dependent on the initial conditions. Cellular membranes are highly complex and dynamic in nature, thus, to investigate even experimentally the structure, function, ligand binding dynamics of integral membrane proteins, the latter should be purified from their native membrane environment. The purification process produces detergent based micelles, or reconstituted, and native nanodiscs with the protein embedded within.[21] The thylakoid membrane is highly complex and dynamic in organization that embeds the photosynthetic apparatus through various important interactions.[22] It has been parametrized in the AMBER Force Field (FF)[23] and contains a variety of lipids: MGDG (44%), DGDG (25%), SQDG (25%), PG (6%)[24]. Due to the complexity of the thylakoid membrane, and the presence of charged lipids within, we have chosen to employ the simpler POPC lipid phase (bilayer, or micelle) in this study. This is a common lipid used in biophysical studies, and widely employed in computational models. The OPLS-UA parameters for POPC[25] ensure accuracy and computational efficiency.[26] In addition, the POPC lipid is neutral, without the need of additional ions for system neutrality. Especially for the protein-micelle simulations, the thylakoid membrane equivalent, instead of POPC, would complicate the simulations.

To compare between POPC and thylakoid membrane behavior, simulations were also run on a patch of OPLS-UA POPC-bilayer[25] and the AMBER thylakoid membrane patch[24]. Both patches contained around 500 lipids and 25000 water molecules (TIP3P[27] for the AMBER FF and TIP4P/2005[28] for the OPLS FF). Production simulations were run for 200ns (POPC, 310K) and 300ns (thylakoid, 303K) with equilibration and production classical MD protocols as described before and in the main manuscript. It is remarkable that POPC-bilayer is equilibrated quickly, while the

thylakoid membrane patch needs considerably larger simulation times for equilibration (i.e. convergence of the Area Per Lipid, APL, **Fig. S4 A**). This would render the all-atom simulations in this study, practically difficult, requiring computational power beyond the norm. It is noted that the employment of the native thylakoid membrane composition in this study could partially affect the protein-lipid interactions,[21] that are however not discussed. It is noted that the partial densities (lipids, waters) are consistent between the two membrane patches, ensuring almost the same hydrophobic environment (dimensions, thickness, density) for the integral CP29, PsbS proteins (**Fig. S4 B**). Minor differences exist in the magnitude of lipid-water hydrogen-bonding interactions (**Fig. S4 C**), as judged by the number of hydrogen bonds determined based on cutoffs for the hydrogen – donor – acceptor angle (30^o) and the donor – acceptor, or hydrogen – acceptor distance (0.35nm). Thus, the crucial Protein-Protein and Protein-Ligand interactions probed herein are adequately sampled in a qualitatively similar hydrophobic environment, as compared to the native thylakoid membranes, but with a tremendous gain in computational efficiency.

REFERENCES

1. G. Das, S. Chattoraj, S. Nandi, P. Mondal, A. Saha, K. Bhattacharyya and S. Ghosh, *Physical Chemistry Chemical Physics*, 2017.
2. R. Y. Patel and P. V. Balaji, *The Journal of Physical Chemistry B*, 2005, **109**, 14667-14674.
3. P. J. Bond, J. M. Cuthbertson, S. S. Deol and M. S. Sansom, *Journal of the American Chemical Society*, 2004, **126**, 15948-15949.
4. M. Fan, M. Li, Z. Liu, P. Cao, X. Pan, H. Zhang, X. Zhao, J. Zhang and W. Chang, *Nature structural & molecular biology*, 2015, **22**, 729-735.
5. V. Daskalakis and S. Papadatos, *Biophysical Journal*, **113**, 2364-2372.
6. J. Mongan, *Journal of computer-aided molecular design*, 2004, **18**, 433-436.
7. H. J. Berendsen, D. van der Spoel and R. van Drunen, *Computer Physics Communications*, 1995, **91**, 43-56.
8. D. Kozakov, D. R. Hall, B. Xia, K. A. Porter, D. Padhorny, C. Yueh, D. Beglov and S. Vajda, *Nat. Protocols*, 2017, **12**, 255-278.
9. C. Dominguez, R. Boelens and A. M. Bonvin, *Journal of the American Chemical Society*, 2003, **125**, 1731-1737.
10. G. Van Zundert, J. Rodrigues, M. Trellet, C. Schmitz, P. Kastritis, E. Karaca, A. Melquiond, M. van Dijk, S. De Vries and A. Bonvin, *Journal of molecular biology*, 2016, **428**, 720-725.
11. E. Roberts, J. Eargle, D. Wright and Z. Luthey-Schulten, *BMC bioinformatics*, 2006, **7**, 382.
12. W. Humphrey, A. Dalke and K. Schulten, *Journal of molecular graphics*, 1996, **14**, 33-38.
13. D. Piovesan, G. Minervini and S. C. Tosatto, *Nucleic acids research*, 2016, **44**, W367-W374.
14. S. Park and K. Schulten, *The Journal of chemical physics*, 2004, **120**, 5946-5961.
15. M. A. Cuendet and O. Michielin, *Biophysical journal*, 2008, **95**, 3575-3590.
16. L. Sutto, S. Marsili and F. L. Gervasio, *Wiley Interdisciplinary Reviews: Computational Molecular Science*, 2012, **2**, 771-779.
17. A. Barducci, G. Bussi and M. Parrinello, *Physical review letters*, 2008, **100**, 020603.
18. G. A. Tribello, M. Bonomi, D. Branduardi, C. Camilloni and G. Bussi, *Computer Physics Communications*, 2014, **185**, 604-613.
19. S. E. Feller, Y. Zhang, R. W. Pastor and B. R. Brooks, *The Journal of chemical physics*, 1995, **103**, 4613-4621.
20. S. Tanizaki and M. Feig, *The Journal of Physical Chemistry B*, 2006, **110**, 548-556.
21. E. Reading, Z. Hall, C. Martens, T. Haghighi, H. Findlay, Z. Ahdash, A. Politis and P. J. Booth, *Angewandte Chemie International Edition*, 2017.
22. F. J. Van Eerden, M. N. Melo, P. W. J. M. Frederix and S. J. Marrink, *Biophysical Journal*, **113**, 2669-2681.
23. W. D. Cornell, P. Cieplak, C. I. Bayly, I. R. Gould, K. M. Merz, D. M. Ferguson, D. C. Spellmeyer, T. Fox, J. W. Caldwell and P. A. Kollman, *Journal of the American Chemical Society*, 1995, **117**, 5179-5197.
24. M. Retegan and D. A. Pantazis, *Journal of the American Chemical Society*, 2017, **139**, 14340-14343.
25. J. P. Ulmschneider and M. B. Ulmschneider, *Journal of Chemical Theory and Computation*, 2009, **5**, 1803-1813.
26. A. Laganowsky, E. Reading, T. M. Allison, M. B. Ulmschneider, M. T. Degiacomi, A. J. Baldwin and C. V. Robinson, *Nature*, 2014, **510**, 172-175.
27. P. Mark and L. Nilsson, *The Journal of Physical Chemistry A*, 2001, **105**, 9954-9960.
28. D. C. Elton and M.-V. Fernández-Serra, *The Journal of chemical physics*, 2014, **140**, 124504.